EPJ Web of Conferences **15**, 02004 (2011)
DOI: 10.1051/epjconf/20111502004

Ab initio molecular-dynamics study of structural and electronic properties of liquid $MgSiO_3$ under pressure

R. Yoshimura, S. Ohmura, and F. Shimojo

Department of Physics, Kumamoto University, Kumamoto 860-8555, Japan

Abstract. The structural and electronic properties of liquid $MgSiO_3$ under pressure are investigated by *ab initio* molecular-dynamics simulations. At ambient pressure, most of Si atoms have the same coordination even in the liquid state as in the crystalline phase, i.e., each Si atom is bonded to two bridging oxygen (BO), i.e., O atoms twofold-coordinated to Si, and two nonbridging oxygen (NBO), i.e., O atoms onefold-coodinated to Si. It is, however, found that the structural defects, such as fivefold- or threefold-coordinated Si atoms, are always formed with the rearrangement of Si-O covalent bonds in the atomic diffusion processes. The population analysis clarifies that maximum of the diffusivity in the pressure dependence results from the increasing of the number of defects under compression.

1 Introduction

The structural and dynamic properties of liquid silicates are of great interest because of the importance in the earth's mantle. In addition, the magnesium-rich silicate minerals olivine and orthopyroxene are the primary constituents of the earth mantle [1], and are also present as major phases in chondrite meteorites and interplanetary dust [2, 3].

Crystalline magnesium silicate ($MgSiO_3$) in ambient conditions has a SiO_4 tetrahedral unit in which each silicon atom is coordinated to four oxygen atoms with single bonds [4]. Under compression, a high-pressure phase appears at a pressure of about 25 GPa. This structure has a SiO_6 octahedral unit. Each Mg atom is coordinated to 12 oxygens with bond lengths ranging from 2.014 to 3.12 Å and O-Mg-O angles ranging from 52.19 to 70.89° [5]. The ideal value of an O-Mg-O angle for a regular MgO_{12} polyhedron is 60°. The small variations in the Si-O distances and the small deviation of the O-Si-O angles from 90° (88.5-91.5°) show that the SiO_6 octahedron is much more regular than the MgO_{12} polyhedron.

Since it would be difficult to clarify the diffusion mechanism in liquid $MgSiO_3$ experimentally, theoretical studies would be needed. However, only a few theoretical studies of atomic diffusion have been reported so far [6], while their crystalline phases have been extensively investigated [7]. Berezhnoi and Boiko [6] have used molecular dynamics (MD) simulations with empirical interatomic potentials to investigate the diffusion mechanism of oxygen ions in $Me_2O{\cdot}SiO_2$ (Me = Li, Na, K, Cs) melts at the temperature of 2000 K. They discussed how the nature of alkali ions affects the structure of transient complexes temporarily formed in alkali silicate systems. Although they proposed a model of the diffusion process, the effects of electronic properties are unclear.

In this paper, we carry out *ab initio* molecular-dynamics (MD) simulations of liquid $MgSiO_3$ under pressure. The atomic forces are obtained quantum mechanically from the electronic-structure calculations. The purpose of our study is to clarify the microscopic mechanism of atomic diffusion in the liquid state from first principles. Although some first principles studies of liquid $MgSiO_3$ under pressure have already been reported [8, 9], we are unaware of investigations of the diffusion mechanism in liquid silicates based on first-principles theories. We discuss how Si-O bonds are exchanged, accompanying the diffusion of atoms in detail. Such findings are important not only for understanding the equilibrium properties of liquid $MgSiO_3$ but also for properties of basic liquids in the earth's mantle.

2 Method of Calculation

In our MD simulations, a system of 120 (24Mg+24Si+72O) atoms in a cubic supercell was used under periodic boundary conditions. The equations of motion for atoms were solved via an explicit reversible integrator [10] with a time step of Δt = 1.2 fs. The atomic forces were obtained from the electronic states calculated by the projector-augmented-wave method [11, 12] within the framework of density-functional theory. The generalized gradient approximation [13] was used for the exchange-correlation energy. The plane wave cutoff energies are 30

and 250 Ry for the electronic pseudowave functions and the pseudocharge density, respectively. The energy functional was minimized using an iterative scheme [14, 15]. Projector functions are generated for the 3s, 3p and 3d states of Mg and Si and the 2s and 2p states of O.

For each pressure (0-200 GPa), the temperature was set to the melting point plus about 500 K. To determine the density of the liquid state under compression, a constant-pressure MD simulation [16] was performed for 2.4 ps at each given pressure. The static and diffusion properties were investigated by MD simulations in the canonical ensemble [17, 18].

Table 1. Pressure P, temperature T, number density ρ used in this study.

P (GPa)	T (K)	ρ (Å^{-3})
0.1	2500	0.068
9.5	2900	0.086
21.1	3300	0.099
48.9	4500	0.113
97.8	5500	0.132
149.1	6000	0.146
198.2	7000	0.156

3 Results and discussion

3.1. Structure factor

Figure 1 shows the pressure dependence of the structure factors of liquid $MgSiO_3$. The solid and dashed lines display the X-ray and neutron structure factors, $S_X(k)$ and $S_n(k)$, respectively. $S_X(k)$ is obtained from the partial structure factors $S_{\alpha\beta}(k)$, shown in Fig. 2, with the X-ray scattering factors, and $S_n(k)$ is calculated from $S_{\alpha\beta}(k)$ with the neutron-scattering lengths. At pressures below 10 GPa, clear peaks exist at about k = 2.0 and 4.4 Å^{-1} in the profiles of $S_X(k)$ and $S_n(k)$. Note that the overall profile of $S_X(k)$ at 0 GPa is consistent with the experimental $S_X(k)$ of the vitreous state [19]. While only $S_n(k)$ has another peak at 3.0 Å^{-1} at lower pressures, the corresponding peak grows in $S_X(k)$ at higher pressures. With increasing pressure, the peak at about k = 4.4 Å^{-1} shifts to smaller k, and merges into the peak at about k = 2.0 Å^{-1} in both $S_X(k)$ and $S_n(k)$. A remarkable feature exhibited in the $S_X(k)$ and $S_n(k)$ is the small peak at about k = 1.2 Å^{-1} at 0 GPa, which means that the spatial correlation exists on an intermediate distance ~ 6 Å. This peak disappears under pressure.

Figure 2 shows the Ashcroft-Langreth partial structure factors $S_{\alpha\beta}(k)$. The pressure dependence of the profiles of $S_X(k)$ and $S_n(k)$ is well understood from $S_{\alpha\beta}(k)$. At 0 GPa, $S_{SiSi}(k)$ has the peak at about k = 1.2 Å^{-1}, which gives the corresponding peak in $S_X(k)$ and $S_n(k)$. At lower pressures, $S_{MgMg}(k)$, $S_{SiSi}(k)$ and $S_{OO}(k)$ have the peak at about k = 2.3 Å^{-1}. Because of the cancellation due to the existence of a negative dip in $S_{MgO}(k)$ and $S_{SiO}(k)$, no clear peak appears in $S_X(k)$ around k = 2.3 Å^{-1}. With increasing pressure, all peaks shift to larger k in $S_{MgMg}(k)$, $S_{SiSi}(k)$ and $S_{OO}(k)$, whereas the negative dip changes only a little in $S_{MgO}(k)$ and $S_{SiO}(k)$. Therefore, the peaks of $S_X(k)$ and $S_n(k)$ grow at the corresponding k when the pressure increases. At higher pressures, the main peak of $S_{MgMg}(k)$ is as high as that of $S_{SiSi}(k)$.

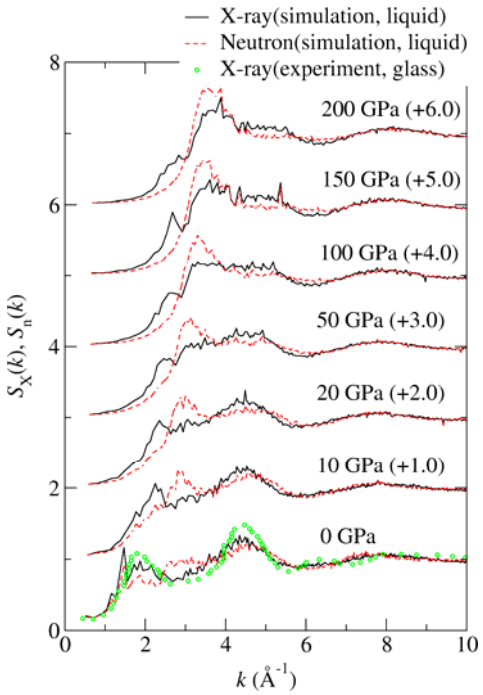

Fig.1. Pressure dependence of the total structure factors. The solid and dashed lines show the X-ray and neutron structure factors, $S_X(k)$ and $S_n(k)$, respectively. The open circles at 0 GPa shows the experimental results for glass $MgSiO_3$. The curves are shifted vertically as indicated by the figures in parentheses.

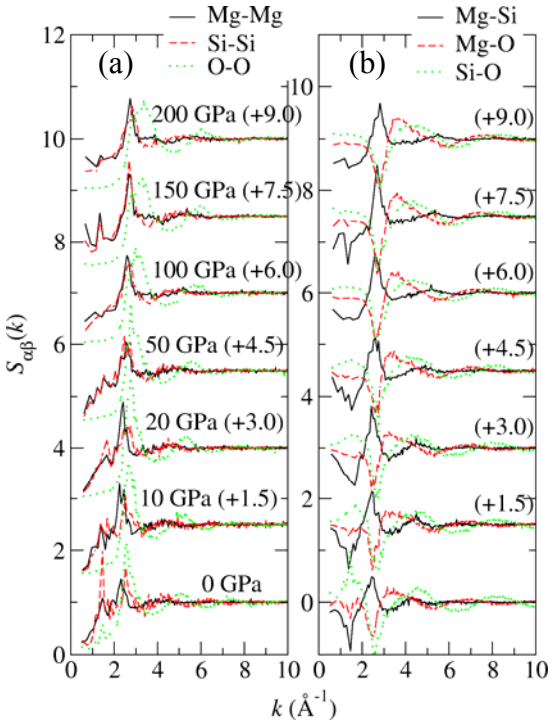

Fig.2. Pressure dependence of the partial structure factors $S_{\alpha\beta}(k)$. (a) The solid, dashed, and dotted lines show $S_{MgMg}(k)$ $S_{SiSi}(k)$, and $S_{OO}(k)$, respectively. (b) The solid, dashed, and dotted lines show $S_{MgSi}(k)$ $S_{MgO}(k)$, and $S_{SiO}(k)$, respectively.

3.2 Diffusivity

The diffusion coefficients D_α for α = Mg, Si, and O atoms are defined as

$$D_\alpha = \lim_{t\to\infty} \frac{1}{6t} \left\langle \left| r_i(t) - r_i(0) \right|^2 \right\rangle ,$$

where $r_i(t)$ is the position of the ith atom at time t. Figure 3 shows D_α as a function of pressure. Whereas D_{Si}, D_O, and D_{Mg} have a maximum at 50 GPa, D_{Mg} has a minimum at 20 GPa. While D_{Mg} has larger values than D_O under pressures up to about 10 GPa, D_O becomes comparable with D_{Mg} at about P = 20 GPa.

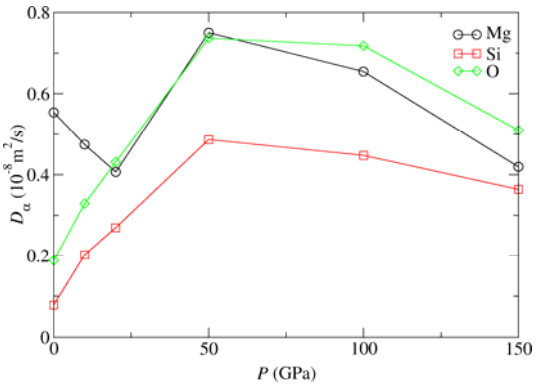

Fig.3. Pressure dependence of the diffusion coefficients D_α for α = Mg (circles), Si (squares) and O (diamonds) atoms.

3.3 Mechanism of atomic diffusion

It is found, from the distribution of coordination numbers, that Si atoms are mainly coordinated to four O atoms; two O atoms bridge two adjacent Si atoms, and the other two O atoms are coordinated to only one Si atom, as in the crystalline phase even though atoms diffuse in the liquid state. However, it is unclear how Si-O bonds are exchanged with the diffusion of atoms in the liquid state while retaining the covalent bonds. To clarify the mechanism of atomic diffusion, we investigate the time evolution of the bonding nature by utilizing population analysis. The bond-overlap population $O_{ij}(t)$, which gives a semiquantitative estimate of the strength of the covalentlike bonding between the ith and jth atoms, is calculated as a function of time.

The diffusion events are shown in figures 4 and 5 where covalent bonds are exchanged around the intermediate defect structure with the fivefold- and sixfold-coordinated Si, respectively. As shown in the top panel of figure 4, $O_{Si\text{-}O1}(t)$ begins to increase at about 67.15 ps, which means that a covalent bond is formed between Si and O1. We can see this new Si-O bond in the snapshot at 67.25 ps. Due to the formation of the bond, Si is overcoordinated to five O atoms. Since the overcoordination is energetically unstable, one of covalent bonds around the fivefold-coordinated Si atom is broken. It is seen that $O_{Si\text{-}O2}(t)$ becomes almost zero for t > 67.70 ps, and the covalent bond between Si and O2 disappears in the snapshot at 67.75 ps.

Above 10 GPa, a number of Si atoms have fivefold coordination as shown in the snapshot at 68.45 ps in the bottom panel of figure 5. $O_{Si\text{-}O1}(t)$ begins to increase at about 68.50 ps, because O1 approaches 'Si' to form a new covalent bond. We can see this new Si-O1 bond in the snapshot at 68.65 ps. Then the octahedron, i.e., sixfold-coordinated Si, is formed. The sixfold coordination is maintained for about 0.2 ps. At 68.8 ps, the Si-O2 bond is broken as $O_{Si\text{-}O2}(t)$ becomes almost zero for t > 68.8 ps.

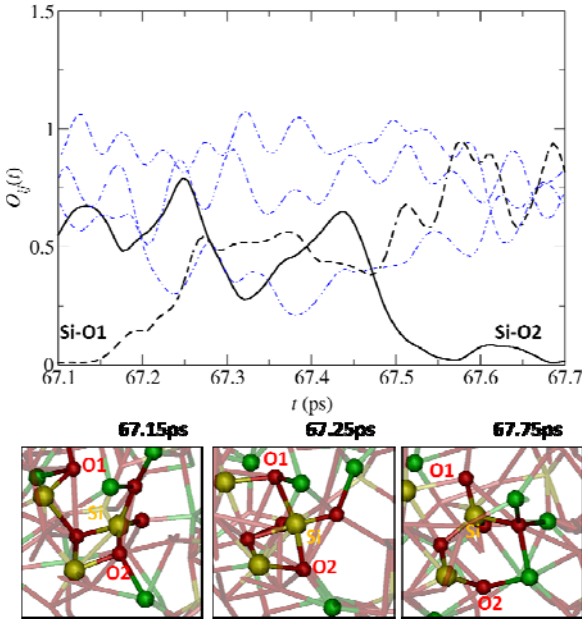

Fig.4. (Top panel) The time evolution of bond-overlap populations $O_{ij}(t)$ for i = Si and j ∈ O in the process of atomic diffusion with transient fivefold-coordinated Si. The thick solid and thick dashed lines show $O_{Si\text{-}O2}(t)$ and $O_{Si\text{-}O1}(t)$, respectively. (Bottom panel) Atomic configurations at t = 67.15, 67.25, and 67.75 ps.

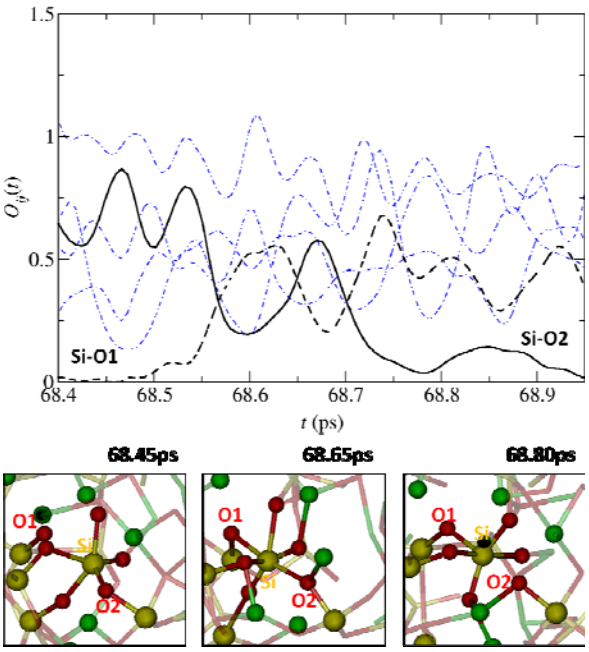

Fig.5. (Top panel) The time evolution of bond-overlap populations $O_{ij}(t)$ for i = Si and j ∈ O in the process of atomic diffusion with transient sixfold-coordinated Si. The thick solid and thick dashed lines show $O_{Si\text{-}O2}(t)$ and $O_{Si\text{-}O1}(t)$, respectively.

(Bottom panel) Atomic configurations at t = 68.45, 68.65, and 68.80 ps.

Figure 6 shows a diffusion event, in which covalent bonds are exchanged around a transient defect structure with threefold-coordinated Si atom. As seen in the top panel of figure 6, initially $O_{\text{Si-O1}}(t)$ and $O_{\text{Si-O2}}(t)$ are almost zero and finite, respectively, for t < 66.55 ps. Note that O1 is overcoodinated to three Si atoms (see the snapshot at 66.55 ps). $O_{\text{Si-O1}}(t)$ and $O_{\text{Si-O2}}(t)$ cross each other at about 66.63 ps, and finally $O_{\text{Si-O2}}(t)$ becomes almost zero, while $O_{\text{Si-O1}}(t)$ is finite for t > 66.7 ps. This means that a covalent-bond exchange occurs around Si: the covalent bond between Si and O1 is broken, and the Si-O2 bond is formed, as seen from the time evolution of $O_{\text{Si-O1}}(t)$ and $O_{\text{Si-O2}}(t)$. Note that the twofold coordination of O1 is recovered after this event. Especially the Si-O bonds except the Si-O1 and Si-O2 bonds are retained while switching the covalent bonds. Around 66.63 ps, the Si atom has threefold coordination with sp^2-like bonding. In this way, the Si-O bonds are exchanged with the formation of undercoordinated Si atoms in liquid $MgSiO_3$. It is, however, necessary to generate adjacent overcoordinated O atoms, such as threefold-overcoordinated O1 in the initial stage of the event.

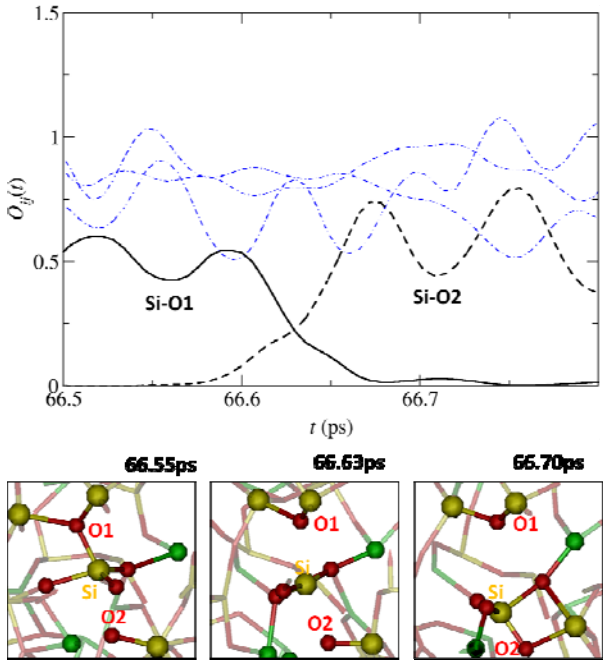

Fig.6. (Top panel) The time evolution of bond-overlap populations $O_{ij}(t)$ for i = Si and $j \in$ O in the process of atomic diffusion with transient threefold-coordinated Si. The thick solid and thick dashed lines show $O_{\text{Si-O1}}(t)$ and $O_{\text{Si-O2}}(t)$, respectively. (Bottom panel) Atomic configurations at t = 66.55, 66.63, and 66.70 ps.

4 Summary

The microscopic mechanism of atomic diffusion in liquid $MgSiO_3$ has been investigated by *ab initio* molecular dynamics simulations. It has been confirmed that, even in the liquid state, silicon atoms are predominantly fourfold-coordinated to hetero atoms with single covalent bonds at ambient conditions, as in the crystalline and vitreous states. We have found that there appears a structural defect whenever atomic diffusion occurs accompanied by the covalent-bond exchanges. The formation mechanism of such defect structure has been discussed in detail using the time evolution of the bond-overlap populations between atoms. The number of structural defects increases gradually with compression. Therefore, atomic diffusion events related to overcoordinated Si occur easily. As a result, D_{Si} and D_{O} increase up to 50 GPa.

Acknowledgments

The authors thank Research Institute for Information Technology, Kyushu University for the use of facilities. The computation was also carried out using the computer facilities at the Supercomputer Center, Institute for Solid State Physics, University of Tokyo.

References

1. G. R. Helffrich and B. J. Wood, Nature **412** (2001) 501
2. F. J. Molster, et. al., Nature **401** (1999) 563
3. J. Dorschner and T. Henning, Astrophys. Rev. **6** (1995) 271
4. Y. Ohashi, Phys. Chem. Miner. **10**, (1984) 217
5. H. Horiuchi, E. Ito, and D. Weidner, Am. Mineral. **72**, (1987) 357
6. G. V. Berezhnoi and G. G. Boiko, Glass Phys. Chem. **31** (2005) 145
7. T. S. Duffy, Rep. Prog. Phys. **68**, (2005) 1811
8. L. Stixrude and B. Karki, Science **310**, (2005) 297
9. J. T. K. Wan, et al., J. Geophys. Res. **112**, (2007) B03208
10. M. Tuckerman, B. J. Berne, and G. J. Martyna, J. Chem. Phys. **97**, (1992) 1990
11. P. E. Blöchl, Phys. Rev. B **49**, (1994) 17953
12. G. Kresse and D. Joubert, Phys. Rev. B **59**, (1999) 1758
13. J. P. Perdew, K. Burke, and M. Ernzerhof, Phys. Rev. Lett. **77**, (1996) 3865
14. G. Kresse and J. Hafner, Phys. Rev. B **49**, (1994) 14251
15. F. Shimojo, R. K. Kalia, A. Nakano, and P. Vashishta, Comput. Phys. Commun. **140**, (2001) 303
16. G. J. Martyna, D. J. Tobias, and M. L. Klein, J. Chem. Phys. **44**, (1966) 3357
17. S. Nosé, Mol. Phys. **52**, (1984) 255
18. W. G. Hoover, Phys. Rev. A **31**, (1985) 1695
19. C. W. Martin, J. B. Chris, A. T. Jean, and S. Sujatha, Chem. Geol. **213**, (2004) 281